

Mechanism and Application of Capacitive-Coupled Memristive Behavior Based on a Biomaterial Developed Memristive Device

Shuangshuo Mao, Xuejiao Zhang, Guangdong Zhou, Yuanzheng Chen, Chuan Ke, Wei Zhou, Bai Sun,* and Yong Zhao*



Cite This: *ACS Appl. Electron. Mater.* 2021, 3, 5537–5547



Read Online

ACCESS |

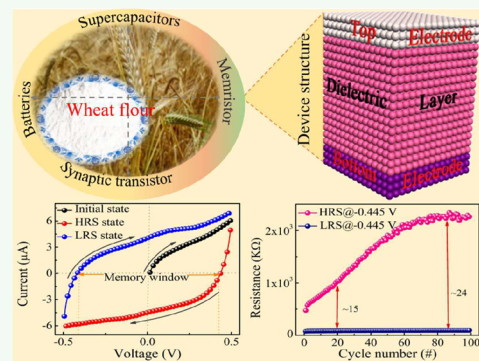
Metrics & More

Article Recommendations

Supporting Information

ABSTRACT: The memory elements are an indispensable part for many electronic equipment and integrated circuit applications. Nonvolatile resistance random access memory (RRAM) based on the memristive effect is considered to be a promising technology in developing memory devices with low cost and high performance. In this work, to meet the development requirements of green and sustainable electronic devices, a functional electronic device is designed and manufactured by using the earth-abundant resources of wheat flour (WF) as the main component of the dielectric layer. The as-prepared bioelectronic device shows a significant capacitive-coupled memristive effect, which has further been studied by changing the mass mixing ratio of WF and polyvinylidene fluoride (PVDF) under different test temperatures. Ultimately, the working mechanism of the bioelectronic device is explained by a conductive filaments model based on a redox reaction. Therefore, this work not only designs and fabricates a bioelectronic device with the capacitive-coupled memristive effect, but also proposes an artificial implantable application for the development of multifunctional bioelectronic devices.

KEYWORDS: capacitive-coupled memristor, resistive switching, conductive filaments, artificial implantable, multifunctional device



1. INTRODUCTION

Today is an era of rapid development with advanced science and technology, greater information circulation, closer communication between people, and more conveniences. Big data is the product of this high-tech era, and it has the characteristics of great numbers, high speed, great diversity, low value density, and much authenticity. At the same time, there are higher requirements for current information memory and processing technology.^{1,2} In order to overcome the challenge of current memory technology, the memristor is considered to be one of the most potential candidates in the field of new concept memory devices.^{3–6} In 1971, the concept of the memristor was first proposed by Chua.⁷ Until 2008, HP Laboratories presented a physical model of memristors with two terminal structures.⁶ Subsequently, the HP lab proposed the logic operation of resistance switching based on memristor devices in 2010.⁸ From then on, the memristor has been widely studied because of it has the advantages of wide application prospects, simple structure, easy fabrication, fast read–write speed, low power consumption, etc.^{9,10} The memristor has usually a sandwich structure, which is composed of top electrode (TE)/dielectric layer/bottom electrode (BE), and the resistance state of the dielectric layer material can be switched between the high resistance state (HRS) and the low resistance state (LRS) during operations.¹¹ The memristor has a wide range of application prospects, mainly including

information storage, logic computing, artificial synapses, and so on.^{12,13}

So far, the memristive effect has been found in many varieties of inorganic and organic materials.^{14–17} Compared with inorganic materials-based memory devices, the organic devices show unique advantages of low cost, light weight, nontoxicity, pollution-free, high flexibility, etc.¹⁸ In addition, organic material based electronic devices can be easily fabricated by self-assembly technology or spin coating methods, which are very suitable for low-cost and large-scale production. Table 1 summarizes some representative organic material prepared memristors, such as silk,¹⁹ chitosan,²⁰ DNA,²¹ albumen,²² pectin,²³ walnut skin,¹¹ and wool keratin.²⁴ Although these materials show considerable memory properties, compared with wheat flour (WF), WF has the advantages of cheap, large quantity, more easily accessible, nontoxic, and completely degraded in organism. WF can be obtained by mechanical processing. Therefore, biomolecular materials have attracted extensive attention due to their unique natural

Received: October 3, 2021

Accepted: December 1, 2021

Published: December 16, 2021

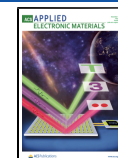


Table 1. Summary of Some Representative Organic Material Based Biomemristors

year	device structure	switching cycles (no.)	retention time (s)	conductive filament model	main physical characteristics	ref
2012	Al/Silk/ITO	~120	>900	yes	resistive switching	19
2015	Pt/Ag-doped chitosan/Ag	~100	>10000	yes	resistive switching	20
2015	Au/(DNA),/Au	~100	>1000000	NO	resistive switching	21
2016	Mg/Albumen/W	~120	>10000	yes	resistive switching	22
2017	Ag/Pectin/FTO	~100	>600	yes	resistive switching	23
2019	Ag/Walnut skin/ITO	~1300	>10000	yes	resistive switching	11
2020	Ag/Wool keratin/ITO			yes	resistive switching	24
2021	Ag/WF@PVDF/FTO	~100	>1000	yes	capacitive-coupled memristive effect	this work

structure and easy acquirement and will become candidate materials for designing biodegradable, environmental-friendly, and sustainable bioelectronic devices. Recently, several memristor devices based on biomaterials have been also studied, for instance, leaves, peel, wood, garlic, etc.^{15,20,23,25,26} In addition to the above-mentioned biomaterials, WF seems to be a promising candidate for memory materials.

WF is one of the most important food crops in the world with an annual output of about 700 million tons.²⁷ In China, amounts of a whopping 14.4 million tons WF were wasted because of necessary processing.²⁸ Therefore, WF powder may become one of the best candidate materials for functional materials, which can be applied the preparation of electronic devices. WF contains starch (72–80%) and protein (8–10%), and it is a green carbon source for the preparation of multistage porous carbon materials.²⁹ Meanwhile, WF is a biodegradable, nontoxic, environmentally friendly, and low consumption polymer electrolyte material with many good properties.³⁰ The hydrogen bond in WF is highly hydrated with water molecules, which is conducive to the transport and storage of water molecules. It has been reported that the solution of WF contains a large number of hydrophilic groups (−OH).³¹ Thus, WF and water molecules have a high degree of hydration in the gelatinization process, and it can also affect ionic conductivity to some extent. Further, the physical properties of WF can be significantly changed when the temperature is higher than 344 K, the water molecules in the system gain enough energy to enter the WF molecules and compete for hydrogen bonds, which can cause hydrogen bonds to break and form microcrystalline bundles of WF molecules.³² Recently, some research works based on WF have been reported, such as synaptic transistors, batteries, supercapacitors, and so on.^{32–34} In particular, Gao et al. have prepared carbon nanotubes using yeast-fermented WF and used it in energy storage.³⁵ Although electronic devices based on WF have been reported, the memory properties of WF have not been reported so far.

In this work, the memristor devices based on the natural biomaterials WF and polymer PVDF compound as the dielectric layer was prepared. The effect of the mass ratio of WF and PVDF on the memory properties of a Ag/WF@PVDF/fluorine-doped tin oxide (FTO) device was also compared. It is found that the memristor devices based on compounds of WF and PVDF show reliable and repeatable memory behavior. This research shows that natural biomaterial based memory devices can help to manufacture environmentally friendly electronic products. This work provides an important step for the development of environmentally friendly, biocompatible, and degradable electronic products.

2. EXPERIMENTAL SECTION

In this experiment, the chemicals and reagents were directly used without further purification, and the WF for the experiment was randomly selected and purchased from the supermarket. The WF main ingredients of flour are starch, protein, fat, and so on. The Ag/WF@PVDF/FTO memristor device was fabricated by using the following steps. First, the conductive substrate with FTO conductive film was cleaned by using deionized water, ethanol, acetone, ethanol, and deionized water in turn 20 min, and it was dried by N₂ gas. Second, the compound powder of WF and PVDF was dissolved in NaClO₄ solution. Third, the obtained mixture in the second step is transferred to the conductive surface of the substrate, and the dielectric layer of memristor is created using spin coating technology; the parameter of spin coating is 600 rpm for 30 s and then 2500 rpm for 30 s. The detailed preparation process is shown in Figure 1a–f.



Figure 1. (a–f) Fabrication process of memristor device. (g) Chemical molecular structure formula of main components in WF. (h) Chemical molecular structure formula of PVDF.

Subsequently, the obtained sample in the third step was dried at room temperature for about 14 h. Finally, a metallic Ag top electrode with diameter of ~1.5 mm was created. Thus, the memristor device was prepared with the Ag/WF@PVDF/FTO structure. The electrical characteristics were tested by an electrochemical workstation (CHI-660E).

3. RESULTS AND DISCUSSION

The detailed preparation process of the Ag/WF@PVDF/FTO memristor is shown in Figure 1a–f, in which the dielectric layer of the memristive device was prepared by a spin-coating method. Figure 1g shows the chemical molecular structure formula of the main components in WF, and the chemical molecular structure formula of PVDF is shown in Figure 1h, in

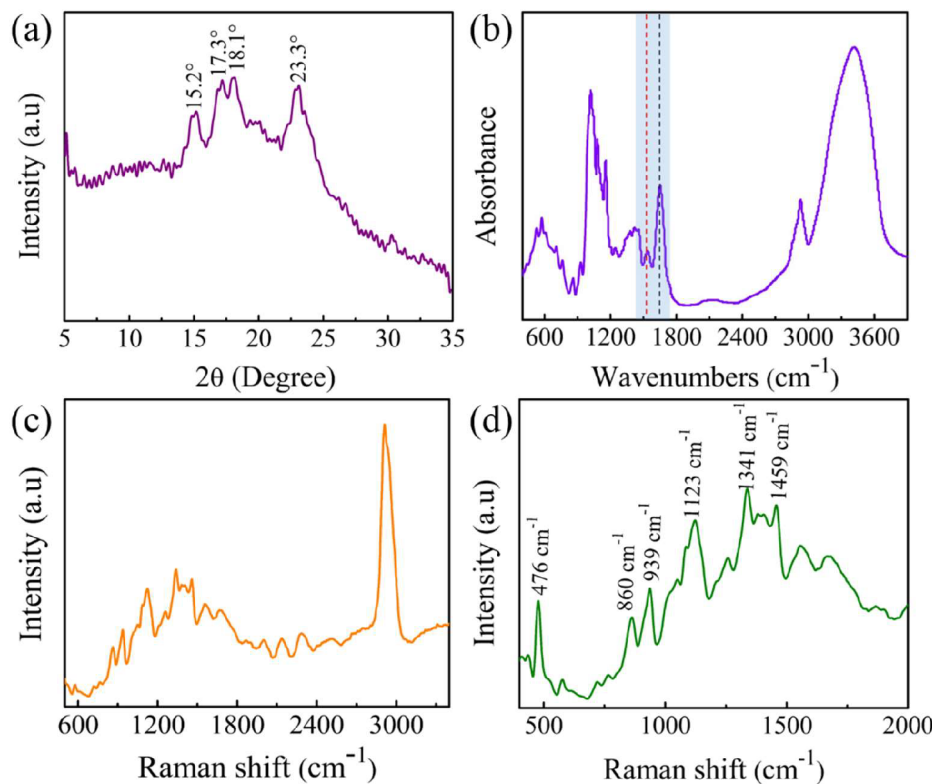


Figure 2. (a) The XRD patterns of pure WF. (b) Infrared spectra of pure WF. (c and d) Raman shift of pure WF.

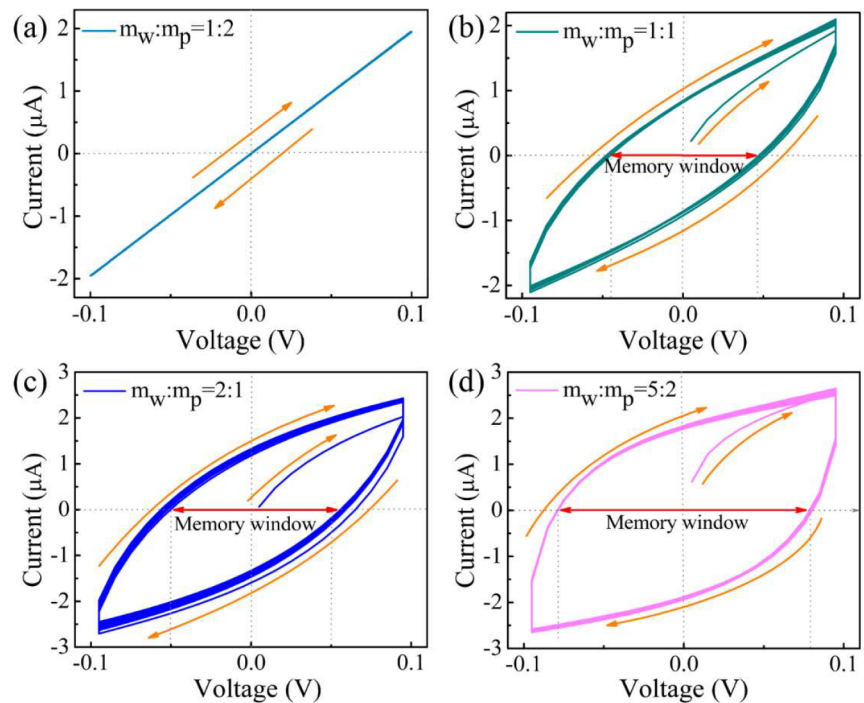


Figure 3. Multicyclic I - V characteristic curve of memristor device with Ag/WF@PVDF/FTO structure for various mass ratios of WF and PVDF. (a) A 1:2. (b) B 1:1. (c) C 2:1. (d) D 5:2.

which it can be seen that the molecular chains are closely arranged with hydrogen bonds. The C–F bond has the properties of a short bond and forms the most stable and firm bond with H^+ . Therefore, PVDF is selected as a binder in this work.

The X-ray diffraction (XRD) pattern of pure WF powder is displayed in Figure 2a. The XRD peak occurs at 15.2° , 17.3° , 18.1° , and 23.3° , showing that the WF has semicrystalline properties, which is consistent with the reported results in the literature.³⁶ In Figure 2b, the infrared spectrum confirmed the existence of a noncovalent hydrogen bond of amide I (1650

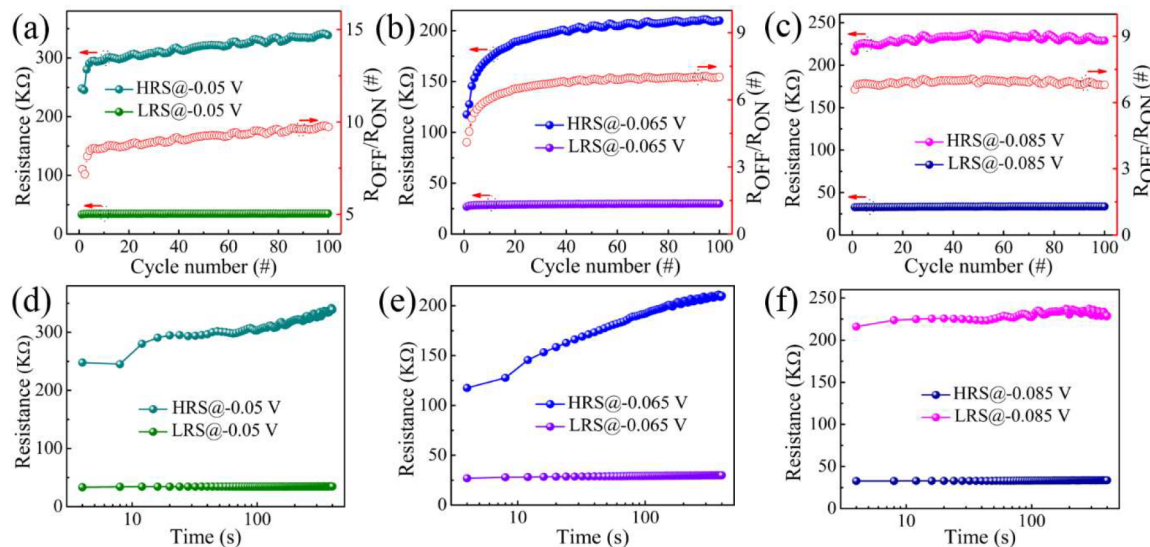


Figure 4. Resistance–cycle number curve and retention test of the Ag/WF@PVDF/FTO memristor device. (a–c) Resistance–cycle number curve of samples B, C, and D. (d–f) Retention test of samples B, C, and D.

cm^{-1} , black dotted line) and amide II (1540 cm^{-1} , red dotted line) in WF, which indicate the hydrogen bonds between amide groups.³⁷ The highest peak is about 3341 cm^{-1} , which is attributed to O–H stretching vibration.³⁸ The existence of –OH group is beneficial to the improvement of proton conductivity. At the same time, it is proven that there are water molecules in WF. The peak near 2930 cm^{-1} is attributed to C–H stretching.³⁸ The Raman shift of WF is presented in Figure 2c and d, in which the Raman spectra of WF displayed some intense peaks (476, 860, 939, and 1341 cm^{-1}) and some small peaks. These high intense peaks are probably related to the stretching vibration of carbohydrate skeleton, which is related to starch, amide I band, and C–O–H mode.^{39,40} The micromorphology of WF powder was characterized by a scanning electron microscope (SEM), as shown in Figure S1.

In this work, memristor device was prepared using a WF and PVDF compound material as the dielectric layer. The PVDF was used as a binder to prevent peeling off of the film during the spin coating process.⁴¹ It was studied that the memory properties are based on different mass ratios of WF and PVDF. In Figure 3, the current–voltage (*I*–*V*) characteristic curves of as-prepared samples were characterized by a CHI-660E electrochemical workstation, which shows the *I*–*V* hysteresis characteristic curves are nonzero crossing when the mass ratio of WF and PVDF exceeds a certain proportion. In the *I*–*V* test process of the Ag/WF@PVDF/FTO device, the direction of applied voltage on the top electrode is $0 \rightarrow 0.1 \rightarrow 0 \rightarrow -0.1 \rightarrow 0 \text{ V}$. To further studying the memory performance of WF and PVDF compound, four devices with various mass ratios (the mass ratio of WF to PVDF is 1:2, 1:1, 2:1, 5:2) as a functional layer were fabricated, and these samples are marked as A, B, C, and D in turn. The *I*–*V* characteristic curve of sample A is shown in Figure 3a, in which it can be seen that the *I*–*V* curve shows a linear relationship without any hysteresis. With the increasing proportion of WF in the compound, the sample B shows an obvious nonzero crossing *I*–*V* hysteresis behavior in Figure 3b. According to previous reports about the capacitance effect in memristor,^{42,43} this nonzero crossing *I*–*V* characteristic curve indicates that it may be formed a capacitive effect in the inside of memristor, and the reason for the formation of

capacitive effect will be discussed in detail later. By comparing the *I*–*V* characteristic curves of samples A and B, we can find that WF plays a very important role for the memory characteristics of memristor device. Further, the *I*–*V* characteristic curves of samples C and D are shown in Figure 3c and d, respectively. As expected, with the increase of WF content in compound, the hysteresis characteristic of *I*–*V* curve becomes more obvious. At the same time, the stability of the device is further improved. Through this study, it can be found that the as-prepared device show obvious capacitive-coupled memristive effect when the amount of WF in the compound exceeds the proportion of 1:2. By changing WF in the mixture proportion, it can be inferred that the capacitive-coupled memristive characteristics of device mainly come from the role of WF from the observed *I*–*V* curve. In previous reports, Zheng et al. defined the memory window by difference value between the positive and negative scanning voltages of capacitance–voltage curves.⁴⁴ Based on the above work, the memory window can be defined by the difference between positive and negative scanning voltage at zero current in the capacitive-coupled memristive effect. Obviously, this memory window is based on charge to storage information. In order to more directly compare maximum HRS/LRS ratio of these as-prepared devices with different proportions WF and PVDF, the *I*–*V* characteristic curves in semilog scale with 100 continuous switching cycles of samples B, C, and D are shown in Figure S2. It can be seen from Figure S2 that the maximal HRS/LRS ratio among the samples B, C, and D are 8, 15, and 9, respectively. Therefore, the WF and PVDF proportion is a crucial impact factor on the memory performance of memristor devices.

To further study the durability and retention characteristics of the Ag/WF@PVDF/FTO memristor device. Each sample was selected an appropriate working voltage to test the durability and stability. The resistance–cycle number and HRS/LRS ratio–cycle curves of samples B, C, and D are shown in Figure 4a, b, and c, respectively. Through comparative study, it is found that the sample D shows relatively good memory performance with outstanding stability. At the same time, the HRS/LRS ratio is relatively

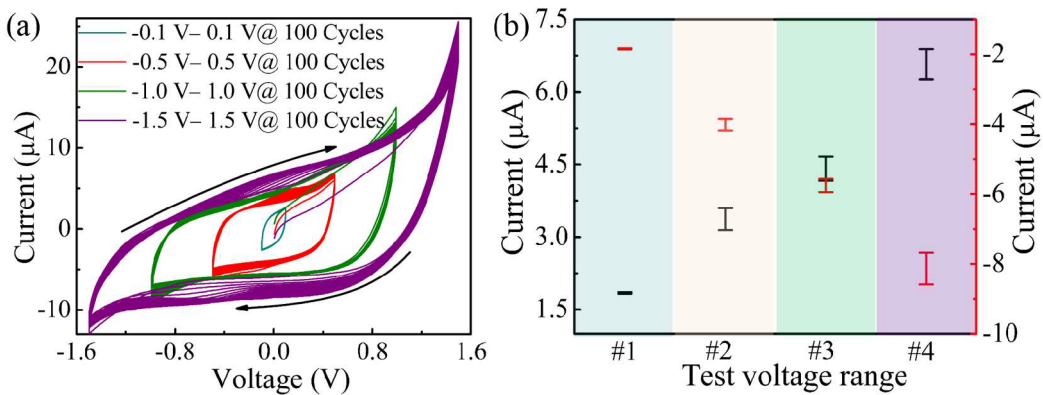


Figure 5. (a) I – V characteristic curves under different scanning voltage ranges. (b) Current distribution at zero bias voltage for different test voltage ranges.

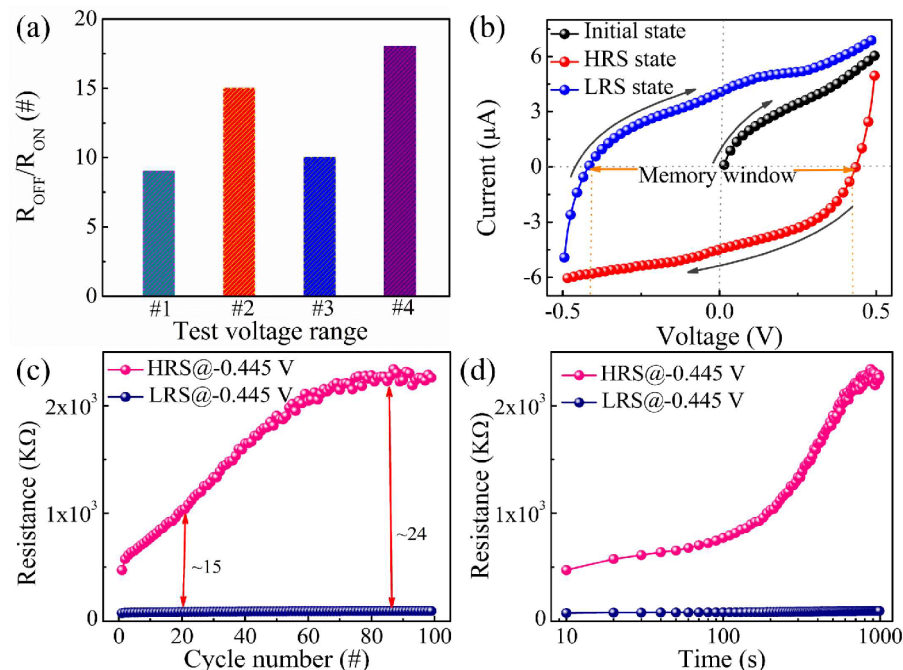


Figure 6. (a) Maximum R_{OFF}/R_{ON} ratio at different test parameters. (b) Typical I – V characteristic curve under no. 2 test parameters. (c) Endurance test of memristors. (d) Retention characteristic of memristors.

stable with the increase of switching cycle number. Figure 4d, e, and f show the retention characteristics of samples B, C, and D devices, respectively. Similarly, the resistance-time of sample D is more relatively stable than others.

The operating voltage range of the memristor device has a certain influence on the performance of the memristive effect.⁴⁵ Considering the HRS/LRS ratio and stability of memristor device with Ag/WF@PVDF/FTO structure, the sample D with good memory performance was further analyzed by setting different scanning voltage ranges. In the process of memory performance test, the range of voltage setting is (1) $-0.1 \rightarrow 0.1$ V, (2) $-0.5 \rightarrow 0.5$ V, (3) $-1.0 \rightarrow 1.0$ V, (4) $-1.5 \rightarrow 1.5$ V, respectively. In each test voltage range, the sweep segments are set at 200. According to this mode, the I – V characteristic curves with continuously switching 100 cycle were obtained, as shown in Figure 5a, in which it can be seen these I – V characteristic curves have obviously attenuation trend with the increase of scanning voltage range. In Figure 5b, the current distributions at zero bias voltage is shown for

different test voltage ranges. With the increase of the test voltage range, the accumulated charges on the surface of the two electrode plates are gradually increased, which leads to the current increase of the absolute value under zero bias voltage. In Figure S3, these typical I – V characteristic curves are displayed on the semilog scale, and the maximal HRS/LRS ratios are displayed for different test parameters 1, 2, 3, and 4, and the corresponding HRS/LRS ratios are 9, 15, 10, and 18 in turn.

In order to more intuitively display the maximum HRS/LRS ratio under different scan voltage ranges, the relationship between the HRS/LRS ratio and the test voltage range is shown in Figure 6a. These parameters should be considered for the practical application of the memristor, including memory window, HRS/LRS ratio, and stability.^{46,47} When the working voltage ranges from -1 to 1 V, the memory performance of sample D can meet the requirement of practical application. The first cycle I – V characteristic curve of sample D is shown in linear scale in Figure 6b, and the initial

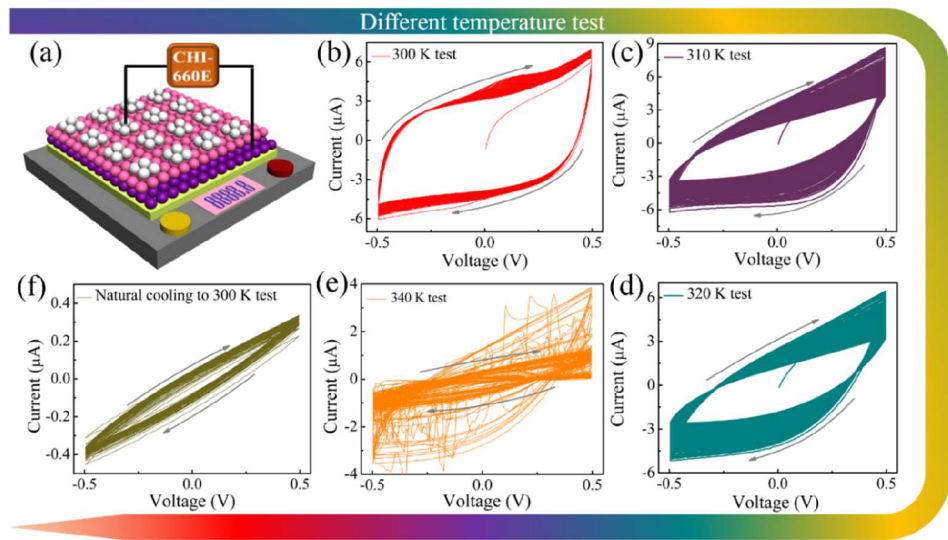


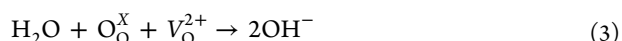
Figure 7. (a) Schematic diagram of test circuit: (b) 300, (c) 310, (d) 320, and (e) 340 K tests. (f) Natural cooling to the 300 K test.

state (IS), HRS, and LRS of I – V characteristic curve were marked using different colors. Black, red, and blue spherical marks represent IS, HRS, and LRS in turn. A large hysteresis I – V characteristic curve with clockwise switch shows the memristor device has a good memory effect. For the practical application of a memory device, the reliability and durability are important factors that should be considered.^{48,49} The endurance performance of a memristor device was characterized by 100 continuous switching cycles of I – V characteristic curves, and the resistance–cycle curve is shown in Figure 6c. When the working voltage of memristor device is set at -0.445 V, the LRS is relatively stable. However, this device faces the same problems as other work that the HRS resistance value is not stable.⁵⁰ In the front 75 switch cycles, the resistance value of HRS gradually increases with the increase of cycle number. When the switching cycles exceeds 75, the resistance value at HRS gradually tends to stability, which displays that the HRS/LRS ratio is ~ 24 . As an important factor to evaluate the performance of nonvolatile memory, the retention performance of the Ag/WF@PVDF/FTO memory devices is presented in Figure 6d.

The I – V characteristic curves of sample D were measured under different temperatures as shown in Figure 7. Figure 7a shows the schematic diagram of the test circuit under different temperatures. In order to study whether temperature can influence the memory performance of the Ag/WF@PVDF/FTO memristor device, the memory performance of sample D was characterized at 300, 310, 320, and 340 K by test cycle I – V curve, as shown in Figure 7b–e, and the I – V curve is shown in Figure 7f when it is cooled to the original temperature again. By comparing with the Figure 7b and f, the dielectric layer surface or micropore moisture content reduces with increase test temperature. The decrease of water content leads to the decrease of H^+ in the memristor, which affects the memory characteristics of the device, especially for the durability. The effect of humidity on memory characteristics will be discussed later. The I – V curves at HRS and LRS for different test temperatures are shown in Figure S4a,b. When the temperature is changed from 300 to 310 K, the resistance values of memristor device at LRS and HRS are reduced. As the testing environment temperature continues to increase, the resistance

value of LRS and HRS are also gradually increased. The reason for this phenomenon may be due to the increase in the number of conductive ions and structural changes in the compound due to the increase of temperature. The loose pores and gaps in the functional layer of the memristor device provide good conditions for the storage of water molecules and the migration of ions.

In previous reports, Valov et al. described the origin of internal electromotive force (V_{emf}), including three parts: Nernst potential (V_N), diffusion potential (V_d), and Gibbs–Thomson potential (V_{GT}).⁵¹ The effect of moisture on low voltage organic field-effect transistors is reported by Kaihovirta et al.⁵² In 2015, Messerschmitt et al. proved for the first time that water has a strong effect on the resistance switching behavior of metal oxides (SrTiO_3) for oxygen anion electronic switch through an experiment model.⁵³ In our previous work, it was confirmed the effect of pH on the memory properties in a biomaterials-based memristor.²⁶ Combining these results obtained from the above works, it is worth noting that biomaterials may be rich in oxygen vacancies. Meanwhile, using spin coating technology prepared films may have many micropores. These micropores in films create good channel for the absorbing of water molecules that come from the atmosphere during testing. For the device with Ag/WF@PVDF/FTO structure, the water molecules may react with oxygen or oxygen vacancies in the lattice of organic materials when the working voltage was applied to the memristor device to produce OH^- , and then the generated OH^- will migrate to the interface between the electrode and dielectric layer under the electric field. The following reactions may occur at the interface between the electrode and the dielectric layer, and the reaction can be described as eqs 1–3.^{54–56}



where O_O^X and V_O^{2+} represent lattice oxygen and oxygen vacancy, respectively. A voltage is applied to the top electrode

of a memristor device, and eqs 1 and 2 or 3 occur. When the above reaction (2) occurs, there will be half-cell reaction, and V_N will be generated originate from the difference of chemical potential between two electrodes and dielectric layer, as can be described in eq 4.⁵¹

$$V_N = V_{S^1} - V_{S^2} = V^0 + \frac{kT}{ze} \ln \frac{(a_{Me^{z+}})_{S^1} (a_{Red})_{S^2}}{(a_{Me})_{S^1} (a_{Ox})_{S^2}} \quad (4)$$

where V_{S^1} and V_{S^2} represent the potential of active electrode/dielectric layer and inert electrode/dielectric layer, respectively. z is the exchange electron number, and V^0 is the standard potentials of different reactions. a_{Red} and a_{Ox} represent the general expression of a redox process. At the same time, the Ag^+ , Na^+ , electrons (e^-), OH^- , and Cl^- ions diffuse in the dielectric layer, and the nonequilibrium diffusion of conductive ions may also cause the diffusion of electromotive force V_d in the device. V_d can be described as eq 5.⁵¹

$$V_d = -\frac{kT}{e} \sum_i \int_{S^2}^{S^1} \frac{t_i}{z_i} d\ln a_i \quad (5)$$

where the k , T , and e are the Boltzmann constant, temperature and elementary charge, respectively. The term a_i represents the ratio of the migration number of a certain cation on the surface between active electrode and inert electrode. Here, z_i represent the charges number. It can be obtained from formula 5 that a larger a_i value can lead to larger V_d values. Thus, the total internal electromotive force (V_{emf}) can be written as eq 6.

$$\begin{aligned} V_{emf} &= V_N + V_d \\ &= V^0 + \frac{kT}{ze} \ln \frac{(a_{Me^{z+}})_{S^1} (a_{Red})_{S^2}}{(a_{Me})_{S^1} (a_{Ox})_{S^2}} \\ &\quad - \frac{kT}{e} \sum_i \int_{S^2}^{S^1} \frac{t_i}{z_i} d\ln a_i \end{aligned} \quad (6)$$

The influence of the surface free energy difference between the metal Ag electrode and the Ag conductive filament can be neglected. Therefore, the Ag/WF@PVDF/FTO device total electromotive force can be written as eq 7.

$$V_{total} = V_{emf} + V \quad (7)$$

V is the voltage value applied to the top electrode of the device in eq 7.

The memristive effect and capacitive effect are coexistence in Ag/WF@PVDF/FTO device. Figure 8a,b shows the typical characteristic curve of the memristive effect and capacitance effect, respectively. The characteristic $I-V$ curve of capacitive-coupled memristive effects is shown in Figure 8c. This nonzero-crossing capacitive-coupled memristive effect can theoretically be realized by a capacitor and a memristor in parallel.⁴² Figure 9a shows the test circuit diagram for the memory performance of the memristor device. In the testing process, a parallel plate capacitor is constructed by a formed space charge region between the electrode and dielectric layer in Figure 9b. The cations and anions accumulate in the two charge regions to form the capacitive effect. As a result, the $I-V$ characteristic of the device is nonzero crossing. Therefore, for the Ag/WF@PVDF/FTO sandwich structure device, it can be regarded as a parallel of a nonlinear resistor with a plate capacitor. The working mechanism can be explained through the formation and fracture of local conductive filaments in the dielectric layer, the conductive filament model is shown in

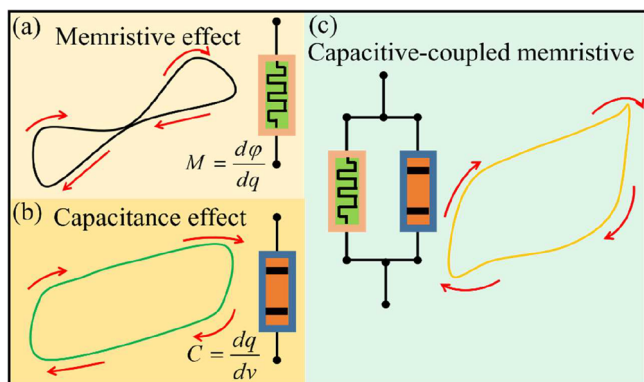


Figure 8. (a) Memristive effect curve. (b) Capacitive effect curve. (c) Capacitive-coupled memristive effect curve.

Figure 9c. When a working voltage is applied to the top electrode of the device, the active Ag electrode initiates reaction according to eq 1, and the Ag atoms on the top electrode are oxidized to Ag ions. Under the action of the electric field, the generated Ag ions will migrate from the top electrode to the bottom electrode along the direction of the electric field. Subsequently, Ag ions are reduced to Ag atoms and stacked locally to form Ag conductive filaments. The formation and fracture of conductive filaments leads to the resistance state that can be switched between LRS and HRS.⁵⁷

Finally, we tried to design a potential application for memristive devices made from the edible biomaterial. For example, gastrointestinal discomfort has become one of the most common health problems in modern society.⁵⁸ Therefore, there is an urgent need for a nontoxic, harmless, and biodegradable electronic device to monitor our health in real time. Although the emerging field of edible electronic products is still in its infancy, it is producing huge scientific repercussions by assuming an economic, effective, safe, and completely natural degradation in the organism after completing its specific functions.⁵⁹ However, it is a great challenge to fabricate a fully edible, nutritious, miniaturized, and multifunctional electronic device.⁵⁸ The materials of edible electronic devices generally include the materials for the preparation of electronic components, the substrate, and packaging materials of devices. Therefore, in this work, WF is used as the functional layer material of electronic devices, and it can be tried to design an edible electronic device. WF is a main food product which can be completely consumed and completely naturally degraded in the body. Therefore, electronic devices made of WF can fully meet the requirements of edible electronic devices. The memristor device with the Ag/WF@PVDF/FTO structure was designed and fabricated in this work. The functional layer of the memristor is WF, which fully meets the requirements of edible devices. If all materials of electronic devices are designed as edible materials, it can be used to monitor human health by taking electronic devices, just like taking medicine. The Ag/WF@PVDF/FTO device exhibits the dual characteristics of memristive and capacitive effects. Because this device has the characteristics of memory and capacitance, combined with other edible electronic components, it can monitor physical health, diagnose and treat diseases, and wirelessly transmit health information to doctors and patients, so that we can take effective measures in time. Figure 10 shows the ideal way to monitor health by taking electronic devices. When we take the electronic device,

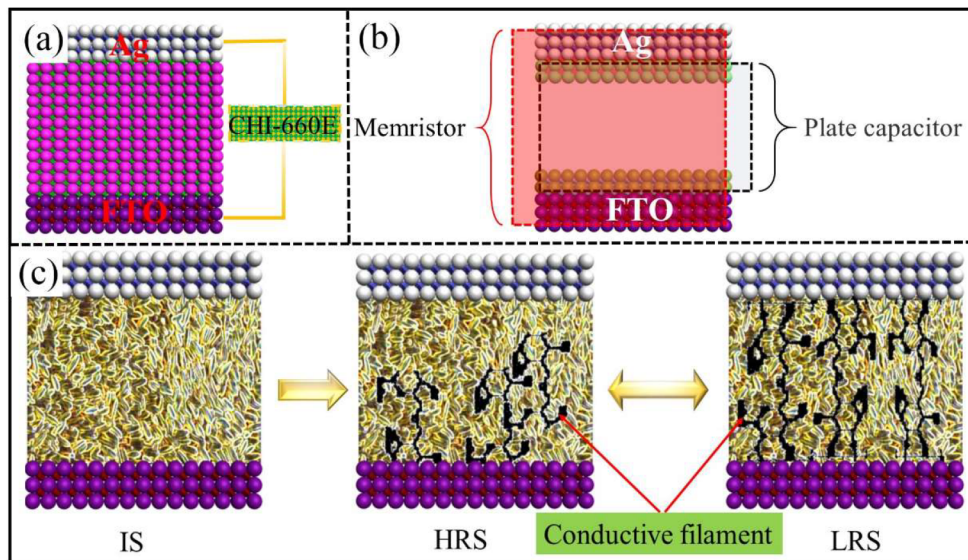


Figure 9. (a) Test circuit for the I – V characteristic curve. (b) Equivalent schematic diagram of the memristor and capacitor. (c) Schematic diagram of the conductive filament model.

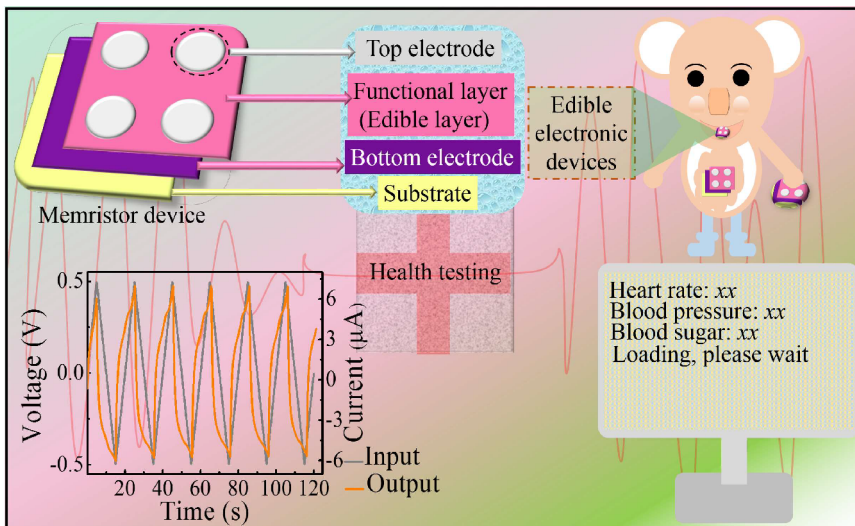


Figure 10. Schematic diagram of the memristor constructed with edible biomaterials to monitor health status.

an input signal is applied to the electronic device in the body, and it will get an output electrical signal. Then, the output signal will be transmitted to the doctor wirelessly. By analyzing these output signals, it can know the health status. Therefore, this work not only prepares and analyzes a device with a memristor coupling capacitor but also points out a method for the development of edible electronic devices.

4. CONCLUSIONS

In conclusion, a memristor device with Ag/WF@PVDF/FTO structure was fabricated by using a WF and PVDF compound as the dielectric layer. Furthermore, the effects of the mass ratio of WF to PVDF and the testing temperature on the memory performance were studied. When a working voltage is applied to the device, some chemical reactions in memristor devices may lead to a nonequilibrium state of the nanoparticles, resulting in the internal electromotive force generated within the device. The formation and fracture of conductive filaments leads to the resistance state that can be switched

between HRS and LRS. Electronic devices with memristive and capacitive dual characteristics may also be one of the development directions of new concept electronic devices in the future. This work provides a guide for the development of multifunctional electronic devices with multiple physical effects.

ASSOCIATED CONTENT

Supporting Information

The Supporting Information is available free of charge at <https://pubs.acs.org/doi/10.1021/acsaem.1c00951>.

Wheat flour powder microscopic characterization and additional memory performance details ([PDF](#))

AUTHOR INFORMATION

Corresponding Authors

Bai Sun — College of Physics and Energy, Fujian Normal University, Fuzhou, Fujian 351007, China; School of Physical Science and Technology, Key Laboratory of

Advanced Technology of Materials and Superconductivity and New Energy R&D Center, Southwest Jiaotong University, Chengdu, Sichuan 610031, China; [ORCID iD](https://orcid.org/0000-0002-5840-509X); Email: bsun@swjtu.edu.cn

Yong Zhao — College of Physics and Energy, Fujian Normal University, Fuzhou, Fujian 351007, China; School of Physical Science and Technology, Key Laboratory of Advanced Technology of Materials and Superconductivity and New Energy R&D Center, Southwest Jiaotong University, Chengdu, Sichuan 610031, China; Email: yzhao@swjtu.edu.cn

Authors

Shuangsoo Mao — College of Physics and Energy, Fujian Normal University, Fuzhou, Fujian 351007, China

Xuejiao Zhang — College of Information Science and Engineering, Hebei North University, Key Laboratory of Biomedical Materials of Zhangjiakou, Zhangjiakou 075000, China

Guangdong Zhou — School of Artificial Intelligence, Southwest University, Chongqing 400715, China; [ORCID iD](https://orcid.org/0000-0002-5824-9488)

Yuanzheng Chen — School of Physical Science and Technology, Key Laboratory of Advanced Technology of Materials, Southwest Jiaotong University, Chengdu, Sichuan 610031, China

Chuan Ke — Superconductivity and New Energy R&D Center, Southwest Jiaotong University, Chengdu, Sichuan 610031, China

Wei Zhou — Department of Electrical & Computer Engineering, University of Waterloo, Waterloo, ON N2L3G1, Canada

Complete contact information is available at:

<https://pubs.acs.org/10.1021/acsaem.1c00951>

Author Contributions

S.M. and B.S. created the idea and designed the study. S.M. fabricated the devices and performed the measurements, X.Z. and G.Z. evaluated the data. All authors performed the analyses. B.S. and Y.Z. supervised the work. B.S. made important revisions. S.M., X.Z., and G.Z. contributed equally. All authors reviewed the manuscript.

Notes

The authors declare no competing financial interest.

ACKNOWLEDGMENTS

The authors gratefully acknowledge financial support from the Sichuan Science and Technology Program (2020YJ0086), Fundamental Research Funds for the Central Universities (2682021CX076), and Basic Research Project of Hebei Province Higher Education (JYT2020028).

REFERENCES

- (1) Wang, Z.; Wu, H.; Burr, G. W.; Hwang, C. S.; Wang, K. L.; Xia, Q.; Yang, J. J. Resistive Switching Materials for Information Processing. *Nat. Rev. Mater.* **2020**, *5*, 173–195.
- (2) Zhou, G.; Sun, B.; Hu, X.; Sun, L.; Zou, Z.; Xiao, B.; Qiu, W.; Wu, B.; Li, J.; Han, J.; Liao, L.; Xu, C.; Xiao, G.; Xiao, L.; Cheng, J.; Zheng, S.; Wang, L.; Song, Q.; Duan, S. Negative Photoconductance Effect: An Extension Function of the TiO_x-Based Memristor. *Adv. Sci.* **2021**, *8*, 2003765.
- (3) Paul, T.; Sarkar, P. K.; Maiti, S.; Chattopadhyay, K. K. Multilevel Programming and Light-Assisted Resistive Switching in a Halide Tunable All-Inorganic Perovskite Cube for Flexible Memory Devices. *ACS Appl. Electron. Mater.* **2020**, *2*, 3667–3677.
- (4) Hu, W.; Zou, L.; Chen, X.; Qin, N.; Li, S.; Bao, D. Highly Uniform Resistive Switching Properties of Amorphous InGaZnO Thin Films Prepared by a Low Temperature Photochemical Solution Deposition Method. *ACS Appl. Mater. Interfaces* **2014**, *6*, 5012–5017.
- (5) Ge, S.; Guan, X.; Wang, Y.; Lin, C.-H.; Cui, Y.; Huang, Y.; Zhang, X.; Zhang, R.; Yang, X.; Wu, T. Low-Dimensional Lead-Free Inorganic Perovskites for Resistive Switching with Ultralow Bias. *Adv. Funct. Mater.* **2020**, *30*, 2002110.
- (6) Sun, B.; Zhou, G.; Sun, L.; Zhao, H.; Chen, Y.; Yang, F.; Zhao, Y.; Song, Q. ABO₃ Multiferroic Perovskite for Memristive Memory and Neuromorphic Computing. *Nanoscale Horiz.* **2021**, *6*, 939–970.
- (7) Chua, L. O. Memristor-The Missing Circuit Element. *IEEE Trans. Circuit Theory* **1971**, *18*, 507–519.
- (8) Borghetti, J.; Snider, G. S.; Kuekes, P. J.; Yang, J. J.; Stewart, D. R.; Williams, R. S. ‘Memristive’ Switches Enable ‘Stateful’ Logic Operations Via Material Implication. *Nature* **2010**, *464*, 873–876.
- (9) Pi, S.; Li, C.; Jiang, H.; Xia, W.; Xin, H.; Yang, J. J.; Xia, Q. F. Memristor Crossbar Arrays with 6-nm Half-Pitch and 2-nm Critical Dimension. *Nat. Nanotechnol.* **2019**, *14*, 35–39.
- (10) Lee, M.-J.; Lee, C. B.; Lee, D.; Lee, S. R.; Chang, M.; Hur, J. H.; Kim, Y.-B.; Kim, C.-J.; Seo, D. H.; Seo, S.; Chung, U.-I.; Yoo, I.-K.; Kim, K. A Fast, High-Endurance and Scalable Non-Volatile Memory Device Made From Asymmetric Ta₂O_{5-x}/TaO_{2-x} Bilayer Structures. *Nat. Mater.* **2011**, *10*, 625–630.
- (11) Mao, S.; Zhang, X.; Sun, B.; Li, B.; Yu, T.; Chen, Y.; Zhao, Y. A Bio-Memristor with Overwhelming Capacitance Effect. *Electron. Mater. Lett.* **2019**, *15*, 547–554.
- (12) Wang, Z.; Rao, M.; Midya, R.; Joshi, S.; Jiang, H.; Lin, P.; Song, W.; Asapu, S.; Zhuo, Y.; Li, C.; Wu, H.; Xia, Q.; Yang, J. J. Threshold Switching of Ag or Cu in Dielectrics: Materials, Mechanism, and Applications. *Adv. Funct. Mater.* **2018**, *28*, 1704862.
- (13) Cheng, L.; Li, Y.; Yin, K.-S.; Hu, S.-Y.; Su, Y.-T.; Jin, M.-M.; Wang, Z.-R.; Chang, T.-C.; Miao, X.-S. Functional Demonstration of a Memristive Arithmetic Logic Unit (MemALU) for In-Memory Computing. *Adv. Funct. Mater.* **2019**, *29*, 1905660.
- (14) Yan, X.; Li, X.; Zhou, Z.; Zhao, J.; Wang, H.; Wang, J.; Zhang, L.; Ren, D.; Zhang, X.; Chen, J.; Lu, C.; Zhou, P.; Liu, Q. Flexible Transparent Organic Artificial Synapse Based on the Tungsten/Egg Albumen/Indium Tin Oxide/Polyethylene Terephthalate Memristor. *ACS Appl. Mater. Interfaces* **2019**, *11*, 18654–18661.
- (15) Park, Y.; Lee, J.-S. Flexible Multistate Data Storage Devices Fabricated Using Natural Lignin at Room Temperature. *ACS Appl. Mater. Interfaces* **2017**, *9*, 6207–6212.
- (16) Guo, T.; Sun, B.; Zhou, Y.; Zhao, H.; Lei, M.; Zhao, Y. Overwhelming Coexistence of Negative Differential Resistance Effect and RRAM. *Phys. Chem. Chem. Phys.* **2018**, *20*, 20635–20640.
- (17) Tao, Y.; Ding, W.; Wang, Z.; Xu, H.; Zhao, X.; Li, X.; Liu, W.; Ma, J.; Liu, Y. Improved Switching Reliability Achieved in HfO_x Based RRAM with Mountain-Like Surface-Graphited Carbon Layer. *Appl. Surf. Sci.* **2018**, *440*, 107–112.
- (18) Zhou, L.; Mao, J.; Ren, Y.; Han, S.-T.; Roy, V. A. L.; Zhou, Y. Recent Advances of Flexible Data Storage Devices Based on Organic Nanoscaled Materials. *Small* **2018**, *14*, 1703126.
- (19) Hota, M. K.; Bera, M. K.; Kundu, B.; Kundu, S. C.; Maiti, C. K. A Natural Silk Fibroin Protein-Based Transparent Bio-Memristor. *Adv. Funct. Mater.* **2012**, *22*, 4493–4499.
- (20) Raeis Hosseini, N.; Lee, J.-S. Resistive Switching Memory Based on Bioinspired Natural Solid Polymer Electrolytes. *ACS Nano* **2015**, *9*, 419–426.
- (21) Qin, S.; Dong, R.; Yan, X.; Du, Q. A Reproducible Write-(Read)_n-Erase and Multilevel Bio-Memristor Based on DNA Molecule. *Org. Electron.* **2015**, *22*, 147–153.
- (22) He, X.; Zhang, J.; Wang, W.; Xuan, W.; Wang, X.; Zhang, Q.; Smith, C. G.; Luo, J. Transient Resistive Switching Devices Made from Egg Albumen Dielectrics and Dissolvable Electrodes. *ACS Appl. Mater. Interfaces* **2016**, *8*, 10954–10960.

- (23) Sun, B.; Zhang, X.; Zhou, G.; Li, P.; Zhang, Y.; Wang, H.; Xia, Y.; Zhao, Y. An Organic Nonvolatile Resistive Switching Memory Device Fabricated with Natural Pectin from Fruit Peel. *Org. Electron.* **2017**, *42*, 181–186.
- (24) Shi, C.; Lan, J.; Wang, J.; Zhang, S.; Lin, Y.; Zhu, S.; Stegmann, A. E.; Yu, R.; Yan, X.; Liu, X. Flexible and Insoluble Artificial Synapses Based on Chemical Cross-Linked Wool Keratin. *Adv. Funct. Mater.* **2020**, *30*, 2002882.
- (25) Sun, B.; Zhu, S.; Mao, S.; Zheng, P.; Xia, Y.; Yang, F.; Lei, M.; Zhao, Y. From Dead Leaves to Sustainable Organic Resistive Switching Memory. *J. Colloid Interface Sci.* **2018**, *513*, 774–778.
- (26) Mao, S.; Sun, B.; Yu, T.; Mao, W.; Zhu, S.; Ni, Y.; Wang, H.; Zhao, Y.; Chen, Y. pH-Modulated Memristive Behavior Based on an Edible Garlic-Constructed Bio-Electronic Eevice. *New J. Chem.* **2019**, *43*, 9634–9640.
- (27) Zhao, H.; Cheng, Y.; Lv, H.; Zhang, B.; Ji, G.; Du, Y. Achieving Sustainable Ultralight Electromagnetic Absorber from Flour by Turning Surface Morphology of Nanoporous Carbon. *ACS Sustainable Chem. Eng.* **2018**, *6*, 15850–15857.
- (28) Yu, P.; Zhang, Z.; Zheng, L.; Teng, F.; Hu, L.; Fang, X. A Novel Sustainable Flour Derived Hierarchical Nitrogen-Doped Porous Carbon/Polyaniline Electrode for Advanced Asymmetric Supercapacitors. *Adv. Energy Mater.* **2016**, *6*, 1601111.
- (29) Yu, P.; Wang, Q.; Zheng, L.; Jiang, Y. Construction of Ultrathin Nitrogen-Doped Porous Carbon Nanospheres Coated With Polyaniline Nanorods for Asymmetric Supercapacitors. *Front. Chem.* **2019**, *7*, 455.
- (30) Youssef, A. M.; El-Sayed, S. M. Bionanocomposites Materials for Food Packaging Applications: Concepts and Future Outlook. *Carbohydr. Polym.* **2018**, *193*, 19–27.
- (31) Raeis-Hosseini, N.; Lee, J.-S. Controlling the Resistive Switching Behavior in Starch-Based Flexible Biomemristors. *ACS Appl. Mater. Interfaces* **2016**, *8*, 7326–7332.
- (32) Yang, Y.; Li, J.; Chen, Q.; Zhou, Y.-H.; Zhu, W.-Q.; Zhang, J.-H. Double-Gate InZnO Synaptic Transistor with Aqueous-Solution-Processed Wheat Flour Electrolyte. *Org. Electron.* **2020**, *77*, 105518.
- (33) Hong, X.; Liu, Y.; Fu, J.; Wang, X.; Zhang, T.; Wang, S.; Hou, F.; Liang, J. A Wheat Flour Derived Hierarchical Porous Carbon/Graphitic Carbon Nitride Composite for High-Performance Lithium-sulfur Batteries. *Carbon* **2020**, *170*, 119–126.
- (34) Wu, X.; Jiang, L.; Long, C.; Fan, Z. From Flour to Honeycomb-Like Carbon Foam: Carbon Makes Room for High Energy Density Supercapacitors. *Nano Energy* **2015**, *13*, 527–536.
- (35) Gao, Z.; Song, N.; Zhang, Y.; Schwab, Y.; He, J.; Li, X. Carbon Nanotubes Derived from Yeast-Fermented Wheat Flour and Their Energy Storage Application. *ACS Sustainable Chem. Eng.* **2018**, *6*, 11386–11396.
- (36) Saiah, R.; Sreekumar, P. A.; Leblanc, N.; Castandet, M.; Saiter, J.-M. Study of Wheat-Flour-Based Agropolymers: Influence of Plasticizers on Structure and Aging Behavior. *Cereal Chem.* **2007**, *84*, 276–281.
- (37) Lei, Z.; Huang, J.; Wu, P. Traditional Dough in the Era of Internet of Things: Edible, Renewable, and Reconfigurable Skin-Like Iontronics. *Adv. Funct. Mater.* **2020**, *30*, 1908018.
- (38) Gao, W. T.; Zhu, L. Q.; Tao, J.; Wan, D. Y.; Xiao, H.; Yu, F. Dendrite Integration Mimicked on Starch-Based Electrolyte-Gated Oxide Dendrite Transistors. *ACS Appl. Mater. Interfaces* **2018**, *10*, 40008–40013.
- (39) Lohumi, S.; Lee, H.; Kim, M. S.; Qin, J.; Cho, B.-K. Raman Hyperspectral Imaging and Spectral Similarity Analysis for Quantitative Detection of Multiple Adulterants in Wheat Flour. *Biosystems Engineering* **2019**, *181*, 103–113.
- (40) Cebi, N.; Dogan, C. E.; Develioglu, A.; Yayla, M. E. A.; Sagdic, O. Detection of L-Cysteine in Wheat Flour by Raman Microspectroscopy Combined Chemometrics of HCA and PCA. *Food Chem.* **2017**, *228*, 116–124.
- (41) Slack, J.; Halevi, B.; McCool, G.; Li, J.; Pavlicek, R.; Wycisk, R.; Mukerjee, S.; Pintauro, P. Electrospun Fiber Mat Cathode with Platinum-Group-Metal-Free Catalyst Powder and Nafion/PVDF Binder. *ChemElectroChem* **2018**, *5*, 1537–1542.
- (42) Sun, B.; Chen, Y.; Xiao, M.; Zhou, G.; Ranjan, S.; Hou, W.; Zhu, X.; Zhao, Y.; Redfern, S. A. T.; Zhou, Y. N. A Unified Capacitive-Coupled Memristive Model for the Nonpinched Current-Voltage Hysteresis Loop. *Nano Lett.* **2019**, *19*, 6461–6465.
- (43) Zhou, G.; Ren, Z.; Sun, B.; Wu, J.; Zou, Z.; Zheng, S.; Wang, L.; Duan, S.; Song, Q. Capacitive Effect: An Original of the Resistive Switching Memory. *Nano Energy* **2020**, *68*, 104386.
- (44) Zheng, Y.; Fischer, A.; Sawatzki, M.; Doan, D. H.; Liero, M.; Glitzky, A.; Reineke, S.; Mannsfeld, S. C. B. Introducing pinMOS Memory: A Novel, Nonvolatile Organic Memory Device. *Adv. Funct. Mater.* **2020**, *30*, 1907119.
- (45) Banerjee, W.; Zhang, X.; Luo, Q.; Lv, H.; Liu, Q.; Long, S.; Liu, M. Design of CMOS Compatible, High-Speed, Highly-Stable Complementary Switching with Multilevel Operation in 3D Vertically Stacked Novel $\text{HfO}_2/\text{Al}_2\text{O}_3/\text{TiO}_x$ (HAT) RRAM. *Adv. Electron. Mater.* **2018**, *4*, 1700561.
- (46) Cao, X.; Han, Y.; Zhou, J.; Zuo, W.; Gao, X.; Han, L.; Pang, X.; Zhang, L.; Liu, Y.; Cao, S. Enhanced Switching Ratio and Long-Term Stability of Flexible RRAM by Anchoring Polyvinylammonium on Perovskite Grains. *ACS Appl. Mater. Interfaces* **2019**, *11*, 35914–35923.
- (47) Li, P.; Zhang, Y.; Guo, Y.; Jiang, L.; Zhang, Z.; Xu, C. Resistance Switching Behavior of a Perhydropolysilazane-Derived SiO_x -Based Memristor. *J. Phys. Chem. Lett.* **2021**, *12* (44), 10728–10734.
- (48) Wang, H.; Hu, L.; Han, W. Resistive Switching Behavior, Mechanism and Synaptic Characteristics in TiO_2 Nanosheets Grown on Ti Plate by Hydrothermal Method. *J. Alloys Compd.* **2021**, *854*, 157200.
- (49) Chen, J.; Feng, Z.; Luo, M.; Wang, J.; Wang, Z.; Gong, Y.; Huang, S.; Qian, F.; Zhou, Y.; Han, S.-T. *J. Mater. Chem. C* **2021**, *9*, 15435–15444.
- (50) Zhou, G.; Ren, Z.; Wang, L.; Sun, B.; Duan, S.; Song, Q. Artificial and Wearable Albumen Protein Memristor Arrays with Integrated Memory Logic Gate Functionality. *Mater. Horiz.* **2019**, *6*, 1877–1882.
- (51) Valov, I.; Linn, E.; Tappertzhofen, S.; Schmelzer, S.; van den Hurk, J.; Lentz, F.; Waser, R. Nanobatteries in Redox-Based Resistive Switches Require Extension of Memristor Theory. *Nat. Commun.* **2013**, *4*, 1771.
- (52) Kaihovirta, N.; Aarnio, H.; Wikman, C.-J.; Wilén, C.-E.; Österbacka, R. The Effects of Moisture in Low-Voltage Organic Field-Effect Transistors Gated with a Hydrous Solid Electrolyte. *Adv. Funct. Mater.* **2010**, *20*, 2605–2610.
- (53) Messerschmitt, F.; Kubicek, M.; Rupp, J. L. M. How Does Moisture Affect the Physical Property of Memristance for Anionic-Electronic Resistive Switching Memories? *Adv. Funct. Mater.* **2015**, *25*, 5117–5125.
- (54) Xia, Y.; Sun, B.; Wang, H.; Zhou, G.; Kan, X.; Zhang, Y.; Zhao, Y. Metal Ion Formed Conductive Filaments by Redox Process Induced Nonvolatile Resistive Switching Memories in MoS_2 film. *Appl. Surf. Sci.* **2017**, *426*, 812–816.
- (55) Torija, M. A.; Sharma, M.; Gazquez, J.; Varela, M.; He, C.; Schmitt, J.; Borchers, J. A.; Laver, M.; El-Khatib, S.; Leighton, C. Chemically Driven Nanoscopic Magnetic Phase Separation at the $\text{SrTiO}_3(001)/\text{La}_{1-x}\text{Sr}_x\text{CoO}_3$ Interface. *Adv. Mater.* **2011**, *23*, 2711–2715.
- (56) Merkle, R.; Maier, J. How Is Oxygen Incorporated into Oxides? A Comprehensive Kinetic Study of a Simple Solid-State Reaction with SrTiO_3 as a Model Material. *Angew. Chem., Int. Ed.* **2008**, *47*, 3874–3894.
- (57) Yang, Y.; Gao, P.; Gaba, S.; Chang, T.; Pan, X.; Lu, W. Observation of Conducting Filament Growth in Nanoscale Resistive Memories. *Nat. Commun.* **2012**, *3*, 732.
- (58) Wu, Y.; Ye, D.; Shan, Y.; He, S.; Su, Z.; Liang, J.; Zheng, J.; Yang, Z.; Yang, H.; Xu, W.; Jiang, H. Edible and Nutritive Electronics:

Materials, Fabrications, Components, and Applications. *Adv. Mater. Technol.* **2020**, *5*, 2000100.

(59) Sharova, A. S.; Melloni, F.; Lanzani, G.; Bettinger, C. J.; Caironi, M. Edible Electronics: The Vision and the Challenge. *Adv. Mater. Technol.* **2021**, *6*, 2000757.

Recommended by ACS

Impact of the Barrier Layer on the High Thermal and Mechanical Stability of a Flexible Resistive Memory in a Neural Network Application

Parthasarathi Pal, Yeong-Her Wang, *et al.*

FEBRUARY 21, 2022

ACS APPLIED ELECTRONIC MATERIALS

[READ !\[\]\(67b99c4d964e257c5482ff1b2462b204_img.jpg\)](#)

A True Random Number Generator Based on Ionic Liquid Modulated Memristors

Bai Sun, Yimin A. Wu, *et al.*

MAY 07, 2021

ACS APPLIED ELECTRONIC MATERIALS

[READ !\[\]\(b52923ac887f6b630066a7f81d758df3_img.jpg\)](#)

High Performance Full-Inorganic Flexible Memristor with Combined Resistance-Switching

Yuan Zhu, Zhen Zhang, *et al.*

APRIL 27, 2022

ACS APPLIED MATERIALS & INTERFACES

[READ !\[\]\(6edc64eef7430608f82cc6c1ef5006c0_img.jpg\)](#)

A Battery-Like Self-Selecting Biomemristor from Earth-Abundant Natural Biomaterials

Bai Sun, Yimin A. Wu, *et al.*

FEBRUARY 02, 2021

ACS APPLIED BIO MATERIALS

[READ !\[\]\(ca98a5155d318582532d305def5ccfdd_img.jpg\)](#)

[Get More Suggestions >](#)